JOURNAL OF CHEMICAL & ENGINEERING DATA

ARTICLE

pubs.acs.org/jced

Measurement of CO_2 Solubility in Ionic Liquids: [BMP][Tf_2N] and [BMP][$MeSO_4$] by Measuring Bubble-Point Pressure

Joon-Hyuk Yim, Ha Na Song, Ki-Pung Yoo, and Jong Sung Lim*

Department of Chemical and Biological Engineering, Sogang University 1 Sinsu-Dong, Mapo-Gu, Seoul, Korea

ABSTRACT: This paper presents the bubble-point pressure data of CO_2 in ionic liquids 1-butyl-1-methyl-pyrrolidinium bis(trifluoromethylsulfonyl)imide ([BMP][Tf_2N]) and 1-butyl-1-methylpyrrolidinium methylsulfate ([BMP][$MeSO_4$]). In our research, the high-pressure phase behavior of carbon dioxide in [BMP][Tf_2N] and [BMP][$MeSO_4$] were observed at pressure up to about 100 MPa in a temperature range from (303.15 to 373.15) K in 10 K intervals by using a high-pressure variable-volume view cell. To investigate the effect of different anion on the solubility of CO_2 in the [BMP] cation based ionic liquids, we compared three [BMP] cation based systems; [BMP][Tf_2N] +, [BMP][TfO] +, and [BMP][$MeSO_4$] + CO_2. In all systems, at lower mole fraction of CO_2 (below 0.3), the solubility is approximately the same, however above 0.3 mol fraction, the ration between pressure and CO_2 mol fraction decreases sharply. Although these experiments have used the same cation, it would appear that the ratio decreases more sharply as the alkyl group chain length of the anion decreases. It can also be observed that when the alkyl group chain lengths are similar, the system containing fluoroalkyl group chain shows higher solubility. However at this stage a thorough analysis of these effects cannot be made. Additionally, the solubility of CO_2 decreases linearly with rising temperatures at a fixed mole fraction of CO_2. The experimental data for the CO_2 + ionic liquid system were correlated using the Peng−Robinson equation of state.

INTRODUCTION

Ionic liquids have garnered an enormous interest over the past few years due to their unique low vapor pressure, which is beneficial for the replacement of traditional organic solvents in organic synthesis and extraction.[1] Ionic liquids can be used as solvents because of their low melting point and because of their ionic structure. When ionic liquids are employed as solvents, superior selectivity is obtained when compared to other conventional organic solvents.

In the past few years, room temperature ionic liquids have been also used as clean solvents and catalysts for green chemistry, as electrolytes for batteries, in photochemistry, and in electrosynthesis. Their potential arises from the necessities of cleaner processes and stronger environmental policies that will be applied.[2] Another application for ionic liquids is their use in separate gas mixtures. Because ILs are nonvolatile, they will not contaminate the gas stream. This quality gives ILs an innate advantage over traditional solvents used for absorbing gases. Whether put to use in conventional absorbers or in supported-liquid membrane systems, ILs as a gas separation medium will require knowledge of the pertinent gas solubilities.[3] They have no significant vapor pressure and thus create no volatile organic pollution during manipulation of industrial operation. Ionic liquids also enable easy separation of organic molecules by direct distillation without loss of ionic liquid. Their liquid range can be as large as 573.15 K, allowing for large reaction kinetic control, which, coupled with their strong solvent properties, allows the minimization of reactor design.[2]

In supercritical fluid extraction, ionic liquid/CO_2 solutions are vital to the recovery of solutes.[4] For these processes, to choose effective ionic liquid for separation, it is important to know the solubility of gas in the ionic liquid we seek to utilize. The supercritical carbon dioxide is the most widely used solvent in various supercritical fluid industries; for example, solvents for extraction, polymer manufacturing, the decaffeination of coffee beans, and so on.[5] This is owing to its nonflammability, nontoxicity, nonpolarity, low critical temperature and pressure values and its affordability. As green solvents, the supercritical carbon dioxide ionic liquids are used in a lot of separation processes.[6]

The purpose of this work is to know the solubility of CO_2 in ionic liquids. We measured the solubility of CO_2 in ILs, 1-butyl-1-methyl-pyrrolidinium bis(trifluoromethylsulfonyl) imide ([BMP][Tf_2N]) and 1-butyl-1-methylpyrrolidinium methylsulfate ([BMP][$MeSO_4$]). The range of temperature for the experimental measurements is from (303.15 to 373.15) K in 10 K intervals. The solubility of CO_2 is determined by measuring the bubble-point pressure at a fixed temperature.

EXPERIMENTAL SECTION

Chemicals. The ionic liquids [BMP][Tf_2N] and [BMP]-[$MeSO_4$] were purchased from C-TRI (Korea). The purity data of [BMP][Tf_2N] and [BMP][$MeSO_4$] are shown in Table 1. The chemical structures of [BMP][Tf_2N] and [BMP][$MeSO_4$] are outlined in Figure 1. The ionic liquid sample was placed

Special Issue: John M. Prausnitz Festschrift

Received: October 26, 2010
Accepted: March 3, 2011
Published: March 14, 2011

Table 1. Purity Data of [BMP][Tf_2N] and [BMP][$MeSO_4$]

ionic liquid	[BMP][Tf2N]	[BMP][$MeSO_4$]
description	colorless liquid	pale yellowish liquid
water contents	32×10^{-6} mass fraction	40×10^{-6} mass fraction
chloride content	15×10^{-6} mass fraction	30×10^{-6} mass fraction
assay	>99%	>99%

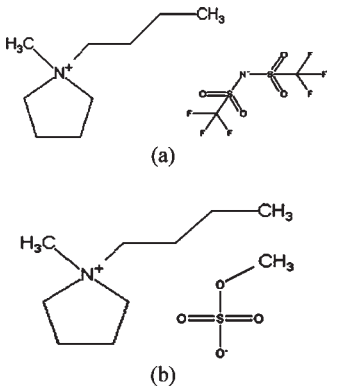

Figure 1. Chemical structure of ionic liquids: (a) [BMP][Tf_2N] and (b) [BMP][$MeSO_4$].

into the high-pressure variable-volume view cell for solubility measurement and evacuated with a vacuum pump at room temperature for several days. Coulometric Karl Fischer titration (Metrohm model 684) was performed on a sample of the evacuated ionic liquid. The high-purity carbon dioxide (99.995%) used for measurements was purchased from Deokyang Gas Co. (Korea). The ionic liquids and CO_2 gas were used without further purification.

Experimental Apparatus. The solubilities of CO_2 in ionic liquids ([BMP][Tf_2N] and [BMP][$MeSO_4$]) were measured with the high-pressure variable-volume view cell. Figure 2 shows a schematic diagram of the experimental apparatus for measuring the solubilities of CO_2 in ionic liquids. The experimental apparatus used in this work was the same as that used in our previous work.[7] The heart of the system is the high-pressure variable-volume view cell. The main feature of using the variable-volume cell apparatus is that it keeps the contents of the cell constant during the experiment. The cell has a dimension of 16 mm i.d. × 70 mm o.d. and an internal working volume of about 31 cm^3. A piston is placed inside the cell to alter the cell volume. A pressure generator (High Pressure Equipment Co. model 50-6-15) is used to pressurize water and therefrom displace the piston. A change in the cell volume causes a change in the system pressure. A sapphire window is inserted into the view cell for visual observation of the cell interior. The system pressure was measured with a high-precision pressure gauge (Dresser Heise model CC-12-G-A-02B, ± 0.05 MPa accuracy, ± 0.01 MPa resolution) placed between the pressure generator and the view cell. The system temperature was measured to within ± 0.1 K with an RTD temperature probe inserted into the cell. A temperature-controlled forced-convection air bath was used to keep the system temperature constant. A visual observation of the interior of the cell through the sapphire window was achieved with a borescope (Olympus model R080-044-000-50) and a CCD camera

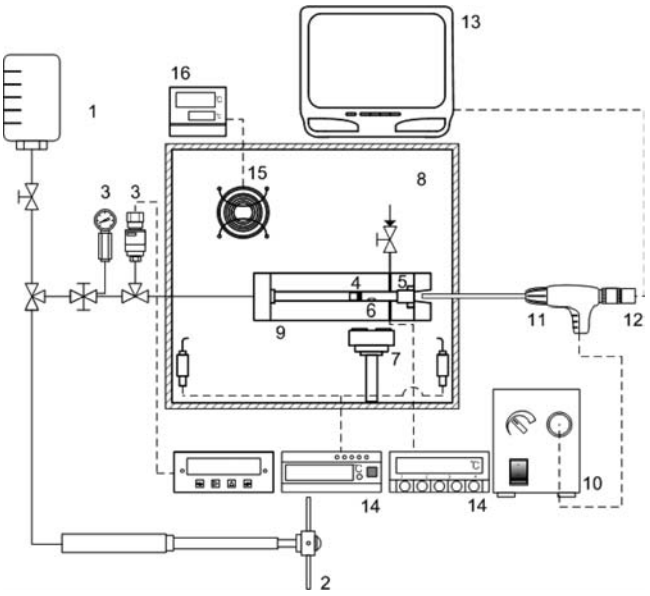

Figure 2. Schematic diagram of the experimental apparatus: (1) Water for pressing; (2) pressure generator; (3) pressure gauge; (4) piston; (5) sapphire window; (6) magnetic bar; (7) stirrer; (8) air bath; (9) variable-volume view cell; (10) light source; (11) borescope; (12) CCD camera; (13) monitor; (14) temperature gauge; (15) heater; (16) heating controller.

connected to a monitor. A magnetic stirring system was equipped under the cell body to mix the contents in the cell. A stirring bar in the cell was activated by a samarium−cobalt magnet located below the cell, and the magnet was driven by an electric motor.

Experimental Procedure. An ionic liquid sample was loaded into the high-pressure variable-volume view cell. The quantity of the sample was about (8 to 9) g. This creates adequate space to agitate the stirring bar in the variable view cell. The piston, stirring bar, and sapphire window are inserted into the variable view cell. A piston creates the space inside the cell with a pressure generator that is used to pressurize water. We observed the cell interior through the sapphire window. To remove any trapped air present in the cell and any dissolved gas and water in the ionic liquid, the cell was evacuated with a vacuum pump at room temperature for several days before the experiment. Once the vapor space of the system was fully evacuated, a known amount of CO_2 was loaded into cell. The exact amount of CO_2 gas introduced into the cell was determined by weighing the CO_2 sample cylinder on a balance (Precias model 1212 M) with an accuracy of ± 1 mg before and after loading. To prevent any loss of CO_2 gas in the feed line during loading, the CO_2 gas in the feed line was recovered back into the CO_2 sample cylinder by dipping the cylinder into a Dewar flask filled with liquid nitrogen. The uncertainties in measuring ionic liquid and CO_2 are (0.2 and 2) mg, respectively. The uncertainty analysis for the composition measurement for each component was performed in accordance with the International Organization of Standardization (ISO) guidelines[8] and was analyzed within ± 0.005 mol fraction for each component. The mole fraction of CO_2 in ionic liquid was calculated on the basis of known quantities of CO_2. To dissolve CO_2 in ionic liquid, the ionic liquid + CO_2 mixture were agitated with a stirring bar. As the pressure increases, CO_2 and ionic liquid mixture in the cell reaches a single phase. The pressure was

Table 2. Critical Properties and Acentric Factor of Ionic Liquids Calculated from Modified Lydersen−Joback−Reid Method[12]

ionic liquids	M/g·mol^{-1}	T_b/K	T_c/K	P_c/MPa	ω
[BMP][Tf_2N]	422.41	833.30	1209.16	2.48	0.32
[BMP][$MeSO_4$]	253.36	706.42	1023.74	3.09	0.42

Table 3. Solubility Data for the [BMP][Tf_2N] + CO_2 System

$x(CO_2)$	T/K	P/MPa	$x(CO_2)$	T/K	P/MPa	$x(CO_2)$	T/K	P/MPa
0.2276	303.15	0.68	0.6176	303.15	4.27	0.8029	303.15	35.16
	313.15	0.99		313.15	5.40		313.15	39.34
	323.15	1.23		323.15	6.80		323.15	44.54
	333.15	1.40		333.15	8.30		333.15	48.40
	343.15	1.56		343.15	9.79		343.15	52.75
	353.15	1.82		353.15	11.50		353.15	56.23
	363.15	2.04		363.15	13.30		363.15	59.44
	373.15	2.26		373.15	14.85		373.15	62.77
0.3500	303.15	1.57	0.6745	303.15	5.85			
	313.15	1.93		313.15	7.48			
	323.15	2.38		323.15	9.74			
	333.15	2.78		333.15	12.06			
	343.15	3.22		343.15	14.75			
	353.15	3.64		353.15	17.13			
	363.15	4.08		363.15	19.82			
	373.15	4.55		373.15	22.72			
0.4776	303.15	2.65	0.7249	303.15	6.80			
	313.15	3.32		313.15	10.83			
	323.15	4.01		323.15	14.70			
	333.15	4.69		333.15	18.00			
	343.15	5.44		343.15	21.83			
	353.15	6.33		353.15	24.61			
	363.15	7.25		363.15	27.79			
	373.15	8.09		373.15	30.71			
0.5431	303.15	3.36	0.7661	303.15	14.86			
	313.15	4.25		313.15	19.78			
	323.15	5.16		323.15	24.67			
	333.15	6.10		333.15	28.52			
	343.15	7.16		343.15	32.80			
	353.15	8.30		353.15	35.76			
	363.15	9.45		363.15	38.59			
	373.15	10.68		373.15	40.80			

subsequently reduced until the first CO_2 bubble was observed from the solution. At this moment, we measured the pressure of the cell and regarded this reading as the bubble-point pressure at a fixed CO_2 mole fraction and temperature. The pressure reduction rates for the determinations of the bubble-point pressure ranged from approximately 0.05 MPa·s^{-1} for the highest bubble-point pressure case to 0.001 MPa·s^{-1} for the lowest bubble-point pressure case. The reduction rate was so slow that the effect of the rate on the results of the bubble-point pressure was not observed. After one set of experiments (from (303.15 to 373.15) K) was finished at a fixed CO_2 mole fraction, more CO_2 was charged into the cell and a CO_2 mole fraction of a new set of experimental system was recalculated. All other experiments having increasing CO_2 mole fractions were performed in this manner. Every measurement was repeated more than three times at each temperature to obtain accurate data. The uncertainty of the temperature measurement was ± 0.1 K and the bubble-point pressure measurement was ± 0.01 MPa.

Table 4. Solubility Data for the [BMP][$MeSO_4$] + CO_2 System

$x(CO_2)$	T/K	P/MPa	$x(CO_2)$	T/K	P/MPa
0.2871	303.15	3.07	0.6049	303.15	76.90
	313.15	3.86		313.15	81.43
	323.15	4.50		323.15	84.60
	333.15	5.23		333.15	87.97
	343.15	6.05		343.15	90.60
	353.15	6.87		353.15	92.95
	363.15	7.75		363.15	95.10
	373.15	8.60		373.15	97.30
0.3970	303.15	7.17			
	313.15	8.20			
	323.15	10.08			
	333.15	12.34			
	343.15	14.80			
	353.15	17.82			
	363.15	20.23			
	373.15	22.68			
0.4833	303.15	12.40			
	313.15	14.89			
	323.15	17.90			
	333.15	20.20			
	343.15	22.72			
	353.15	25.10			
	363.15	27.53			
	373.15	29.50			
0.5319	303.15	22.40			
	313.15	30.27			
	323.15	26.45			
	333.15	33.80			
	343.15	36.76			
	353.15	39.40			
	363.15	42.20			
	373.15	45.85			

MODELING

The experimental (CO_2 +ionic liquid) data were correlated with the Peng−Robinson equation of state (PR-EoS).[9]

To calculate the parameters of the PR-EoS, critical temperature (T_c), critical pressure (P_c), and acentric factor (ω) of both components CO_2 and ionic liquids were needed. Those properties of CO_2 are easily obtained from the literature,[10] however, such information on ionic liquids are not available. Therefore, critical properties of ionic liquids have to be estimated. To estimate the critical properties of ionic liquids in this work, we employed a modified Lydersen-Joback-Reid method:[11,12] a group contribution method known to yield a relatively good result especially for molecules

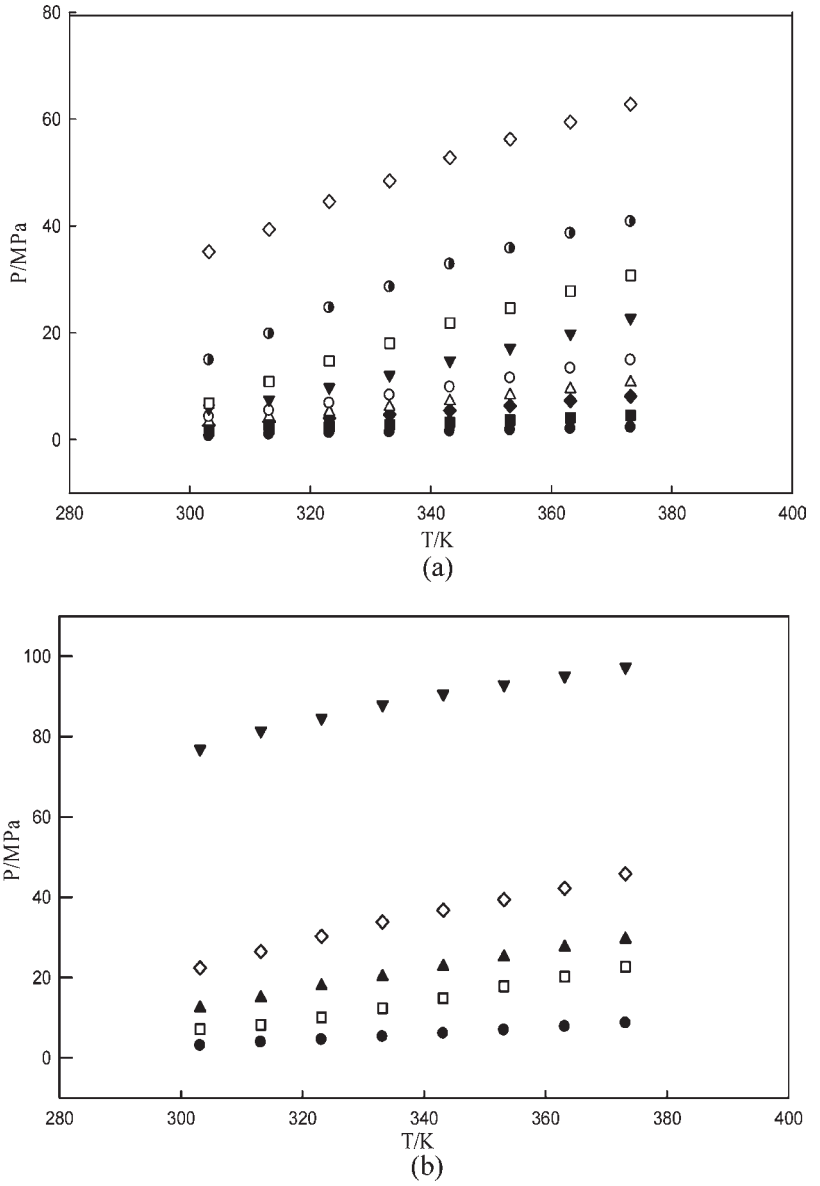

Figure 3. $P-T$ diagram of CO_2 solubilities of the CO_2 + ionic liquid system at different CO_2 mole fraction: (a) CO_2 + [BMP][Tf_2N]: ●, 0.2276; ■, 0.3500; ♦, 0.4776; Δ, 0.5431; ○, 0.6176; ▼, 0.6745; □, 0.7249; ◑, 0.7661; and ◊, 0.8029. (b) CO_2 + [BMP][$MeSO_4$]: ●, 0.2871; □, 0.3970; ▲, 0.4833; ◊, 0.5319; ▼, 0.6049.

with high molecular weights.[12]

$$T_b/\mathrm{K} = 198.2 + \sum n\Delta T_{bM} \quad (1)$$

$$T_c/\mathrm{K} = \frac{T_b}{0.5703 + 1.021\sum n\Delta T_M - (\sum n\Delta T_M)^2} \quad (2)$$

$$P_c/\mathrm{bar} = \frac{M}{[0.2573 + \sum n\Delta P_M]^2} \quad (3)$$

where M is the molecular weight in ionic liquid. Groups considered for the modified Lydersen−Joback−Reid method are presented in the literature.[11]

The acentric factor is calculated as[11]

$$\omega = \frac{(T_b - 43)(T_c - 43)}{(T_c - T_b)(0.7T_c - 43)} \log\left[\frac{P_c}{P_b}\right] - \frac{(T_c - 43)}{(T_c - T_b)} \log\left[\frac{P_c}{P_b}\right] + \log\left[\frac{P_c}{P_b}\right] - 1 \quad (4)$$

The acentric factor is calculated by critical properties and normal boiling temperature (T_b for P_b = 0.1 MPa). All the calculated critical properties, the normal boiling temperature and acentric factors of ionic liquids are listed in Table 2.

RESULTS AND DISCUSSION

In this work, high-pressure phase behavior of carbon dioxide in [BMP][Tf_2N] and [BMP][$MeSO_4$] were measured in a

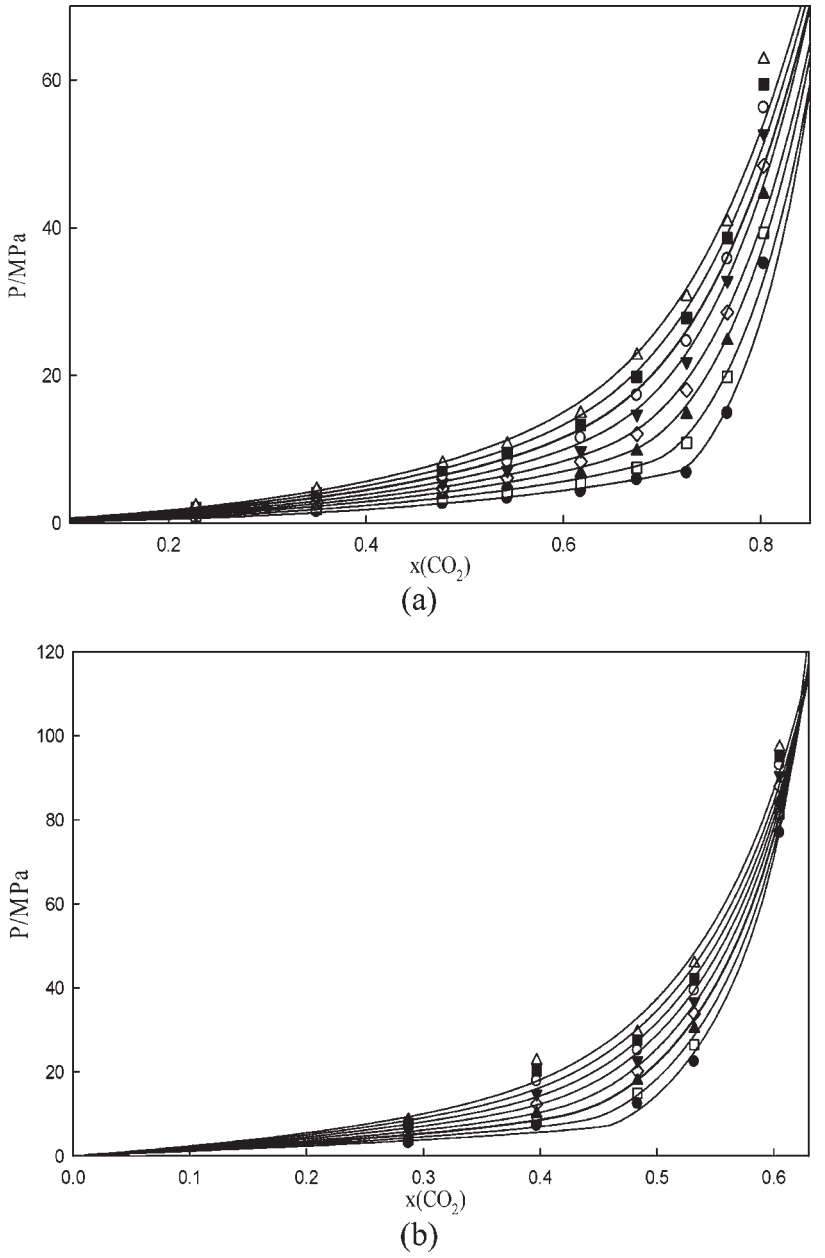

Figure 4. $P-x_1$ diagram of the (a) CO_2 + [BMP][Tf_2N] and (b) CO_2 + [BMP][$MeSO_4$] at different temperatures: ●, 303.15 K; □, 313.15 K; ▲, 323.15 K; ◇, 333.15 K; ▼, 343.15 K; ○, 353.15 K; ■, 363.15 K; and Δ, 373.15 K. The lines are the calculations by the PR-EoS model. The binary interaction parameters for each temperature are listed in Table 5.

temperature range from (303.15 to 373.15) K in 10 K intervals. The experimental results of the carbon dioxide + [BMP][Tf_2N] system are presented in Table 3, and those of the carbon dioxide + [BMP][$MeSO_4$] system are presented in Table 4, respectively. Figures 3a,b and 4a,b also show their bubble-point pressures versus the temperature and CO_2 mole fraction, respectively. As can be seen in Figure 3, the bubble-point pressure increases linearly with increasing temperature at a fixed CO_2 mole fraction. This means that at a fixed pressure, the solubility of CO_2 in ionic liquid decreases commensurate to rises in temperature. Additionally, at a fixed CO_2 mole fraction, the CO_2 solubility in ionic liquid is dramatically affected by temperature. Figure 4 shows that as the CO_2 mole fraction increases, the bubble-point pressures increase dramatically. So the slope of the solubility pressure with temperature increased steeply with increases in CO_2 mole fraction while the bubble-point pressures increased with increasing CO_2 mole fraction at a fixed temperature.

Calculated binary interaction parameters from (303.15 to 373.15) K in 10 K intervals for each system are given in Table 5. The calculated results from the PR-EoS with mixing rules are illustrated in Figure 4 along with the experimental data. The correlation model successfully predicts the solubility pressure data at lower mole fraction of CO_2. When mole fraction of CO_2 increases, however, the deviation between experimental data and calculated results grows. Deviations between experimental and calculated values were shown in Table 6. We calculated the average absolute deviation in percentage (AAD %) for each

system. The average value of the AAD % of [BMP][$MeSO_4$] was two times higher than that of [BMP][Tf_2N]. As the temperature increase, the AAD % values of [BMP][Tf_2N] decreased. Whereas the AAD % values of [BMP][$MeSO_4$] are similar in most temperature ranges.

Table 5. Binary Interaction Parameters for the Ionic Liquids System

	[BMP][Tf_2N]		[BMP][$MeSO_4$]	
T/K	k_{12}	l_{12}	k_{12}	l_{12}
303.15	0.0788791	0.0585427	0.1021482	0.0030404
313.15	0.0784086	0.0526179	0.1093185	0.0065809
323.15	0.0798268	0.0514217	0.1160921	0.0095643
333.15	0.0812601	0.0534481	0.1231325	0.0128493
343.15	0.0839507	0.0562193	0.1282109	0.0143671
353.15	0.0840051	0.0563844	0.1343326	0.0168562
363.15	0.0849332	0.0577421	0.1401772	0.0189060
373.15	0.0857307	0.0593948	0.1475717	0.0220204

Table 6. Average Absolute Deviations (AAD %) between Experimental Data and Calculated Value for the [BMP][Tf_2N] + CO_2 and [BMP][$MeSO_4$] + CO_2 System

	AAD %[a]	
T/K	[BMP][Tf_2N]	[BMP][$MeSO_4$]
303.15	7.28	12.37
313.15	7.35	9.97
323.15	7.34	11.24
333.15	7.01	12.62
343.15	6.49	13.55
353.15	6.34	13.60
363.15	5.86	13.14
373.15	5.69	12.57
average	6.67	12.38

[a] Average absolute deviation in percentage: AAD% = $(1/N)\Sigma_{i=1}^{N}(|P_i^{calc} - P_i^{exp}|)/(P_i^{exp}) \times 100$ (N = number of data).

Figure 5 compares the solubility data for the [BMP][Tf_2N] + CO_2, [BMP][TfO] + CO_2[7] and [BMP][$MeSO_4$] + CO_2 systems at 333.15 K. This shows the effect of different anion on the solubility of CO_2 in the [BMP] cation based ionic liquids. As can be seen in this figure, at lower mole fraction of CO_2 (below $0.3x_1$), the solubility of CO_2 in different ionic liquids is almost the same. But over than $0.3x_1$, the solubility of CO_2 shows completely different tendency. Among these three systems, [BMP][Tf_2N] + CO_2 system shows the lowest bubble-point pressures, [BMP][TfO] + CO_2 system shows middle, and [BMP][$MeSO_4$] + CO_2 system shows the higest bubble-point pressures in the entire mole fraction. It means that the solubility of CO_2 is the highest in [BMP][Tf_2N] and [BMP][TfO][7] is medium, and [BMP][$MeSO_4$] is the lowest. Figure 5 also illustrate that solubility of CO_2 increase as the fluoroalkyl group chain length increases and as the CO_2 mole fraction increases, the bubble-point pressures increase dramatically.

CONCLUSIONS

The solubility of CO_2 in ionic liquids [BMP][Tf_2N] and [BMP][$MeSO_4$] were determined by measuring the bubble-point pressures of the binary mixtures using high pressure variable volume view cell. The solubility of CO_2 in ionic liquids [BMP][Tf_2N] and [BMP][$MeSO_4$] were observed from (303.15 to 373.15) K in 10 K intervals. Normal boiling temperature, acentric factor and critical properties of ionic liquids were estimated with a modified Lydersen−Joback−Reid method. PR-EoS and mixing rules were used to calculate the solubility pressure. To investigate the effect of different anion on the solubility of CO_2 in the [BMP] cation based ionic liquids, we compared three [BMP] cation based systems; [BMP][Tf_2N] +, [BMP][TfO] +, and [BMP][$MeSO_4$] + CO_2. In all systems, at lower mole fraction of CO_2 (below 0.3), the solubility is approximately the same, however above 0.3 mol fraction, the ration between pressure and CO_2 mol fraction decreases sharply. Although these experiments have used the same cation it would

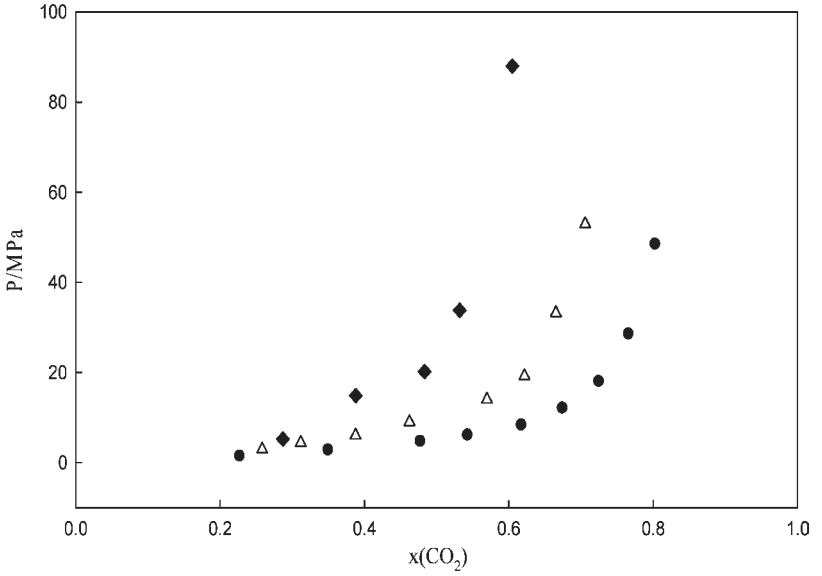

Figure 5. Comparison of $P-x_1$ graph of CO_2 solubilities in the [BMP] based ionic liquids systems at 333.15 K: ●, [BMP][Tf_2N]; Δ, [BMP][TfO] (our previous work);[7] and ♦, [BMP][$MeSO_4$].

dx.doi.org/10.1021/je101100d |J. Chem. Eng. Data 2011, 56, 1197–1203

appear that the ratio decreases more sharply as the alkyl group chain length of the anion decreases. It can also be observed that when the alkyl group chain lengths are similar, the system containing fluoroalkyl group chain shows higher solubility. However at this stage a thorough analysis of these effects cannot be made, and the solubility of CO_2 decreases linearly with rising temperatures at a fixed mole fraction of CO_2.

AUTHOR INFORMATION

Corresponding Author

*Tel.: +82-2-705-8918. Fax: +82-2-705-7899. E-mail: limjs@sogang.ac.kr.

Funding Sources

This work was supported by the Special Research Grant of Sogang University.

REFERENCES

(1) Renken, A.; Hessel, V.; Lob, P.; Miszczuk, R.; Uerdingen, M.; Kiwi-minsker, L. Ionic liquid synthesis in a microstructured reactor for process intensification. *Chem. Eng. Process.* **2007**, *46*, 840–845.

(2) Gota., I.; Gonzalez-Olmos, R.; Iglesias, M.; Medina, F. New short aliphatic chain ionic liquids: Synthesis, Physical properties and catalytic activity in aldol condensation. *J. Phys. Chem . B* **2007**, *111*, 12468–12477.

(3) Anthony, J. L.; Maginn, E. J.; Brennecke, J. F. Solubilities and thermodynamic properties of gases in the ionic liquid 1-n-butyl-3-methylimidazolium hexafluorophosphate. *J. Phys. Chem. B* **2002**, *106*, 315–320.

(4) Visser, A. E.; Swatloski, R. P.; Reichert, W. M.; Griffin, S. T.; Rogers, R. D. Traditional extractants in nontraditional solvents: groups 1 and 2 extraction by crown ethers in room-temperature ionic liquids. *Ind. Eng. Chem. Res.* **2000**, *39*, 3596–3604.

(5) Ari, Y.; Sako, T.; Takebayashi, Y. *Supercritical Fluids: Molecular Interactions, Physical Properties, and New Applications*; Springer Verlag: Berlin, 2001.

(6) Blanchard, L. A.; Brennecke, J. F. Recovery of Organic Products from Ionic Liquids Using Supercritical Carbon Dioxide. *Ind. Eng. Chem. Res.* **2001**, *40*, 287–292.

(7) Song, H.-N.; Lee, B.-C.; Lim, J. S. Measurement of CO_2 Solubility in Ionic Liquids: [BMP][TfO] and [P14,6,6,6][Tf_2N] by Measuring Bubble-Point Pressure. *J. Chem. Eng. Data* **2010**, *55*, 891–896.

(8) *Guide to the Expression of Uncertainty in Measurement*; International Organization of Standardization (ISO): Geneva, Switzerland, 1995.

(9) Peng, D. Y.; Robinson, D. B. A New Two-Constant Equation of State. *Ind. Eng. Chem. Fundam.* **1976**, *15*, 59.

(10) McLinden, M. O.; Klein, S. A.; Lemmoon, E. W.; Peskin, A. P. *Thermodynamic Properties of Refrigerants and Refrigerant Mixtures Database (REFPROP), V.6.01*; NIST: Gaithersburg, MD, 1998.

(11) Valderrama, J. O.; Sanga, W. W.; Lassús, J. A. Critical properties, normal boiling temperature, and acentric factor of another 200 ionic liquids. *Ind. Eng. Chem. Res.* **2008**, *47*, 1318–1330.

(12) Valderrama, J. O.; Robles, P. A. Critical properties, normal boiling temperatures, and acentric factors of fifty ionic liquids. *Ind. Eng. Chem. Res.* **2007**, *46*, 1338–1344.